INTERNATIONAL JOURNAL FOR NUMERICAL METHODS IN FLUIDS
Int. J. Numer. Meth. Fluids 2014; **76**:450–470
Published online 5 August 2014 in Wiley Online Library (wileyonlinelibrary.com). DOI: 10.1002/fld.3941

RESEARCH PAPER PRESENTED AT MULTIMAT 2013:
MULTI-MATERIAL HYDRODYNAMICS SIMULATIONS

Toward a reduction of mesh imprinting

T. B. Lung*,† and P. L. Roe

Department of Aerospace Engineering, University of Michigan, Ann Arbor, MI 48108, USA

SUMMARY

This paper is the initial investigation into a new Lagrangian cell-centered hydrodynamic scheme that is motivated by the desire for an algorithm that resists mesh imprinting and has reduced complexity. Key attributes of the new approach include multidimensional construction, the use of flux-corrected transport (FCT) to achieve second order accuracy, automatic determination of the mesh motion through vertex fluxes, and vorticity control. Toward this end, vorticity preserving Lax–Wendroff (VPLW) type schemes for the two-dimensional acoustic equations were analyzed and then implemented in a FCT algorithm. Here, mesh imprinting takes the form of anisotropic dispersion relationships. If the stencil for the LW methods is limited to nine points, four free parameters exist. Two parameters were fixed by insisting that no spurious vorticity be created. Dispersion analysis was used to understand how the remaining two parameters could be chosen to increase isotropy. This led to new VPLW schemes that suffer less mesh imprinting than the rotated Richtmyer method. A multidimensional, vorticity preserving FCT implementation was then sought using the most promising VPLW scheme to address the problem of spurious extrema. A well-behaved first order scheme and a new flux limiter were devised in the process. The flux limiter is unique in that it acts on temporal changes and does not place *a priori* bounds on the solution. Numerical results have demonstrated that the vorticity preserving FCT scheme has comparable performance to an unsplit MUSCL-H algorithm at high Courant numbers but with reduced mesh imprinting and superior symmetry preservation.

Received 28 February 2014; Revised 16 June 2014; Accepted 1 July 2014

KEY WORDS: acoustic; Lagrangian; multidimensional; Lax–Wendroff; vorticity; flux-corrected transport, flux limiting

1. INTRODUCTION

The numerical simulation of compressible, multi-material flows is a challenging problem that is often suited to Lagrangian methods. Traditionally, most Lagrangian codes have employed staggered storage. Wilkins constructed the first multidimensional staggered Lagrangian algorithm [1] which many workers have improved upon. See, for example, the so-called compatible hydro methods of Caramana *et al.* [2]. However, in the last decade, attention has turned toward cell-centered algorithms due in large part to the successful work of Després and Mazeran [3] and Maire *et al.* [4]. More recent examples of cell-centered algorithm publications include the work of Maire and Breil [5], Carré *et al.* [6], Barlow and Roe [7] and Burton *et al.* [8]. Despite these successes with the cell-centered approach, some old difficulties remain. Continuing areas of interest include mesh imprinting, symmetry preservation, limiting mechanisms, mesh movement, and spurious vorticity. To address these issues, we seek to implement a new cell-centered approach that is multidimensional

*Correspondence to: T. B. Lung, Department of Aerospace Engineering, University of Michigan, Francois-Xavier Bagnoud Aerospace Building, Room 2001, 1320 Beal Avenue, Ann Arbor, MI 48109, USA.
†E-mail: tblung@umich.edu

in nature, utilizes flux-corrected transport (FCT) to achieve second order accuracy, automatically defines mesh motion through vertex fluxes, and implements vorticity control. In combination, these features represent a radical departure from the current practice in both the staggered-grid and cell-centered camps.

Early cell-centered Lagrangian solvers borrowed from standard Eulerian practice by solving one-dimensional Riemann problems at cell faces (see, e.g., [9]). In our opinion, this leads to a major disadvantage in both Eulerian and Lagrangian algorithms in that the physics involved is merely one-dimensional. Acoustic waves are driven by the pressure gradient and velocity divergence. In one dimension, the velocity divergence is indistinguishable from its gradient, however, this is not the case in two or three dimensions. A traditional Godunov-type approach cannot properly account for the velocity divergence in higher dimensions, resulting in the computation of incorrect waves and the inability to respect multidimensional symmetries. In fact, it has been shown that the fluxes of velocity through a face must be derived by averaging fluxes evaluated at its vertices [10–12]. Vertex fluxes cannot be evaluated by supposing the interactions between cells to proceed pairwise, as when solving Riemann problems. Instead, all of the cells meeting at that vertex must be considered.

There is another major disadvantage with a Godunov-type approach that arises in the Lagrangian case: Riemann solutions provide information about the motion of the cell edges, whereas a Lagrangian solver must know how to move the cell vertices. In general, the vertex motion cannot be inferred from the supposed motion of the edges. Després and Mazeran [3] were the first to tackle this difficulty by formulating a method in terms of corner fluxes. Here, a node-based solver computes the flux through the corner of each cell adjacent to the node and a unique nodal velocity in a single step. The success of this work has lead to a fundamental shift in the way cell-centered Lagrangian schemes are constructed as evidenced by the more recent papers cited in the first paragraph. However, it is our view that improvements may still be possible. For example, the node-based solvers in current use introduce complexity by way of additional nodal pressures and do not completely eliminate the reliance on one-dimensional physics.

Development of a new and improved Lagrangian hydrodynamics algorithm with the stated attributes from scratch would be an ambitious goal. Instead of using the nonlinear Euler equations and moving grids as the starting point for this research, a more gradual approach has been adopted. This paper will deal with the acoustic equations in two spatial dimensions and investigate a class of Lax–Wendroff (LW) type methods that are particularly suited to a Lagrangian context. The full set of LW methods for the acoustic problem has four free parameters and includes variants in which the fluxes are evaluated at either edges or vertices or both. We will also consider LW-like schemes that use the same nine-point stencil, but are only first order accurate. Among these are methods that would reduce to classical first order upwinding in one dimension, although they have a perfectly symmetrical appearance. This is possible because of the fact that both the acoustic and Lagrangian equations have equal wave speeds in all directions. Therefore, despite appearances, we are not abandoning the upwinding concept.[‡] The extension of these methods to three dimensions is straightforward. The test environment is further described in Section 2.

There are two central crises associated with the Lax–Wendroff type methods that we seek to resolve. The first crisis, dealt with in Section 3, is the tendency of the mesh to imprint itself on the solution and the associated failure to preserve symmetry. Here, we seek an algorithm that can accurately maintain circular symmetry when the solution is computed on a square mesh. There are, of course, other ways in which the symmetries of the mesh and the solution might be in conflict, but we believe that this simple instance is representative. In [10], the preservation of vorticity is shown to require similar treatment on both square and unstructured grids. The second crisis, resulting from the second order accuracy of the methods, is the need for a nonlinear limiter to prevent spurious extrema from entering the solution. The limiter must be multidimensional and effective in situations where no rigorous definition of monotonicity exists. The limiting crisis will be addressed in Section 4. Numerical results are included in Section 5, and finally, conclusions are drawn in Section 6.

[‡]Upwind schemes employ a dissipation matrix $\underline{Q} = \underline{R}|\underline{\Lambda}|\underline{L}$. If all of the eigenvalues have the same absolute value λ, then $|\underline{\Lambda}| = \lambda \underline{I}$ and $\underline{Q} = \lambda \underline{I}$. We then have a central scheme.

DOI: 10.1002/fld

Some explanation of notation is needed before proceeding. Standard central differencing and averaging operators will be used throughout. They are denoted by δ and μ, respectively, and the result of an operator is located half way in between the input values. The definition for each operator is

$$\mu_x()_{j,k} = 0.5[()_{j+1/2,k} + ()_{j-1/2,k}] \qquad \delta_x()_{j,k} = [()_{j+1/2,k} - ()_{j-1/2,k}]$$
$$\mu_y()_{j,k} = 0.5[()_{j,k+1/2} + ()_{j,k-1/2}] \qquad \delta_y()_{j,k} = [()_{j,k+1/2} - ()_{j,k-1/2}]$$

Vector quantities are denoted by bold face font, while matrices are underlined. Superscripts appearing in discretizations denote the time level, while subscripts refer to spatial indices. Because all meshes are square, $\Delta x = \Delta y \equiv h$, and the Courant number is defined as $\nu = a_0 \Delta t / h$.

2. TEST ENVIRONMENT

As noted in the introduction, we are interested in solving the acoustic equations in two spatial dimensions. Written in conservation form and using subscripts to denote partial differentiation, the governing equations are written

$$\mathbf{U}_t + \mathbf{F}_x + \mathbf{G}_y = 0 \tag{1}$$

where $\mathbf{U} = (\frac{p^*}{\rho_0 a_0^2}, \frac{u^*}{a_0}, \frac{v^*}{a_0})^T \equiv (p, u, v)^T$, $\mathbf{F} = (a_0 u, a_0 p, 0)^T$, and $\mathbf{G} = (a_0 v, 0, a_0 p)^T$. The variables p^*, u^*, and v^* represent perturbations of the fluid properties from a uniform, stationary background state given by ρ_0, p_0, and a_0. These equations are just the linearized version of the Lagrangian system and therefore a natural setting to investigate variations of numerical technique. A formal justification of this was presented in [13]. Additionally, the equations are still intrinsically multidimensional in that there are two spatial dimensions and the flow physics are driven by the velocity divergence and pressure gradient.

To solve the acoustic system, the family of LW schemes that can be derived on a nine point stencil were employed. The scheme that we initially preferred was the rotated Richtmyer (RR) scheme [14], which was shown to exactly preserve compact vorticity, $\boldsymbol{\zeta} = \mu_y \delta_x v - \mu_x \delta_y u$, by Morton and Roe [10]. The RR scheme was of interest not only due to the vorticity preservation property but also because it has a Lagrangian friendly structure. When used to solve the acoustic equations, the RR scheme can be viewed as a linearized Lagrangian method. To better understand the connection, first consider the general update procedure followed by the RR method for two-dimensional acoustics:

1. Using the four neighboring cell-centered values, $\mathbf{U} = (p, \mathbf{V})^T$, compute vertex fluxes, $\hat{\boldsymbol{f}} = (a_0 \mathbf{V}, a_0 p)^T$, at each node.
2. Evolve each vertex flux through one half time step.
3. Update the cell-centered variables by integrating the fluxes around a cell-centered control volume with the Trapezium rule.

A Lagrangian algorithm would look remarkably similar if we take the view that the Eulerian form of the equations will be solved on a mesh that moves with the fluid velocity. This is to say that instead of working with the Lagrangian form of the gas dynamic equations, the advective terms will be subtracted from the Eulerian form. This view point leads to an algorithm that is nearly identical. The acoustic variables are exchanged for momentum, $\mathbf{m}$, and total energy, E and the fluxes become $\hat{\boldsymbol{f}} = (p, p\mathbf{V})^T$. A step can then be added between 2 and 3 in which the mesh is moved. The nodal velocities can be conveniently defined through the vertex fluxes as $\mathbf{V}_{i,j} = (p\mathbf{V})_{i,j} / p_{i,j}$. It should be stressed that the fluxes are defined pointwise at each vertex (not at cell corners) with a unique velocity *and* pressure. Perhaps, it is preferable to think of the fluxes, then, as integration points. Conservation is naturally retained with this approach and the pointwise nature of the fluxes eliminates the possibility of computing the fluxes using pairwise interactions. One-dimensional Riemann solutions will never make an appearance. Figure 1 helps to illustrate the general structure of the

DOI: 10.1002/fld

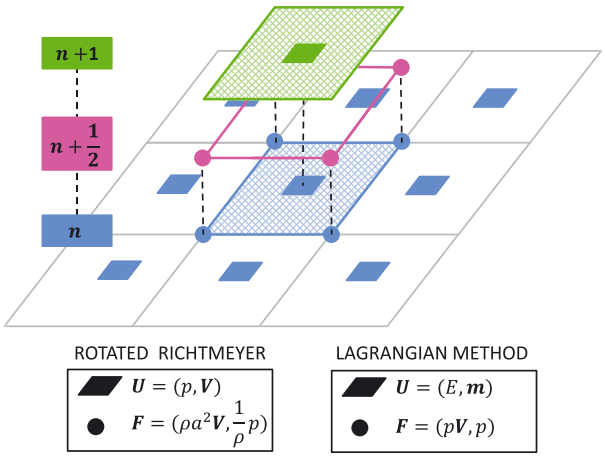

Figure 1. Illustration to reinforce the connection between the RR scheme and its Lagrangian analog. The primary difference in the case of a Lagrangian algorithm is the need to move the mesh. Note that unique nodal velocities can be defined from the nodal fluxes.

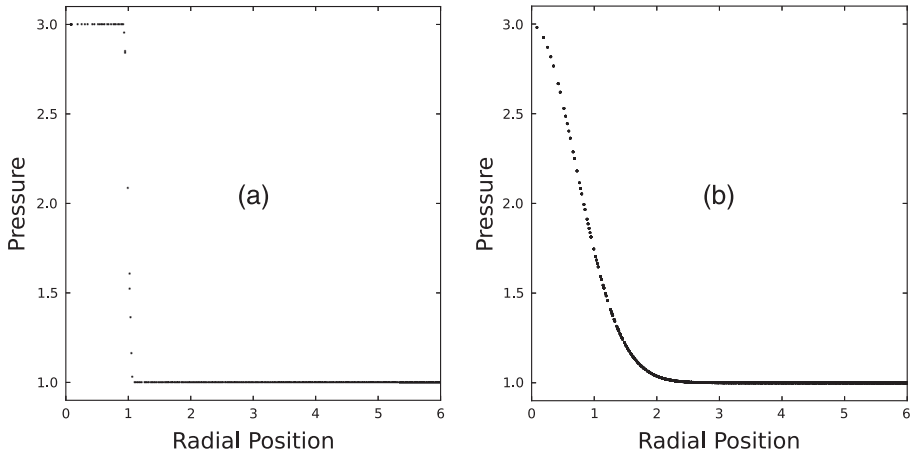

Figure 2. Initial pressure distribution for the discontinuous test problem (a) and smooth test problem (b).

algorithms under consideration and the link between the RR scheme used for acoustics and a full Lagrangian algorithm.

In his investigation of Lax–Wendroff variants, Turkel [15] recommended against using the RR variant 'because of large phase errors'. However, his analysis related only to the case of a scalar problem, or, equivalently, a problem with commuting matrices, and in that case, we can reproduce his analysis and agree with his conclusions. The optimum parameters for a LW scheme do depend on the problem being solved.

The primary test problem utilized in the test environment was a discontinuous, radially symmetric pressure perturbation applied to a fluid at rest. The initial conditions were defined on the domain $x \in [-6, 6]$ and $y \in [-6, 6]$ and set as

$$\begin{array}{ll} p = 2 \text{ if } r \leqslant 1 & u = 0 \\ p = 0 \text{ if } r > 1 & v = 0 \end{array} \qquad a_0 = 1.$$

We also considered a smooth problem in which the discontinuous pressure distribution was replaced by the Gaussian profile

$$p(x, y, 0) = 2 \exp\left[-\left(x^2 + y^2\right)\right]. \tag{2}$$

DOI: 10.1002/fld

The problems were solved on a 100×100 mesh unless otherwise noted. See Figure 2 for plots of the initial pressure distributions. The test problems were useful for a number of reasons. First, the solutions should have perfect radial symmetry, and any deviation from this is easily observed by plotting the data as a function of radius.[§] Second, the resulting system of waves includes a pressure expansion that implodes at the origin and an outgoing compression wave. The shape of the waves changes over time. Third, the vorticity is zero initially and therefore should remain zero for all time. This makes detecting spurious vorticity especially straightforward. Finally, in the case of the discontinuous problem, the ability of numerical methods to handle high frequency data is tested. Now that the test environment and problems have been established, the mesh imprinting and symmetry preservation crisis may be considered.

3. CRISIS I: MESH IMPRINTING AND SYMMETRY PRESERVATION

3.1. Vorticity control

Dukowicz and Meltz [16] implemented a correction procedure to remove unwanted vorticity from the final computed solution. Though expensive and first order, this was successful at reducing mesh imprinting and spurious vorticity generation when solving the Saltzmann test problem. It would, therefore, be desirable to find a scheme that has built in vorticity control. This makes the RR scheme a good place to start. Three questions arise here that we would like to address. First, is spurious vorticity generation a large concern for algorithms that are derived in the absence of any vorticity considerations? Second, can the link between vorticity control and mesh imprinting be established in the context of the acoustic equations and the LW family of schemes? Third, is vorticity control alone an adequate method to preserve symmetry?

Numerical results from the RR scheme and the original LW method were compared using the discontinuous test problem. Contour plots of compact vorticity, rendered at $t = 3$, make a strong case that problems with vorticity will exist if no special care is taken. Figure 3 shows that a substantial amount of vorticity was generated by the original LW scheme in a pattern that is aligned with the mesh and located near the initial pressure discontinuity. In comparison, the RR scheme has properly maintained zero vorticity to double precision. The computations were run with $\nu = 0.6$.

While the improvement demonstrated by RR with respect to vorticity is desirable, changes in mesh imprinting and isotropy are of keen interest. To gauge the effect of vorticity control on these issues, the pressure and velocity magnitude profiles were plotted as a function of radius. See Figure 4, which also includes a reference solution computed using standard methodology (an unsplit MUSCL-Hancock [17] scheme on a 600×600 grid). Two things become evident. First, the RR scheme produces a solution that is much more isotropic than the LW method. This is encouraging, but some slight scatter is still noticeable, especially in the velocity results near the origin. Second, when compared to the reference solution in the background, both the RR and LW schemes produce a number of spurious features. This is to be expected for a discontinuous problem, however, because no limiting was employed. In this section, our objective is solely to obtain the most isotropic solutions possible. The discussion on limiting is left for Section 4. Figure 5 shows results from the smooth, low frequency test problem. We see that in this case, the LW, RR, and the MUSCL-H reference solutions are all nearly the same. The high frequency dispersion relationships for each scheme and the resulting performance on the discontinuous test problem are of primary interest.

While it has been demonstrated that the RR scheme is superior to the original LW scheme with respect to vorticity control and mesh imprinting, further improvements to the method may be possible. The entire family of Lax–Wendroff type schemes was parameterized and investigated to explore this possibility.

[§]This is a much more sensitive test than plotting pressure contours in x, y and judging how circular they look.

DOI: 10.1002/fld

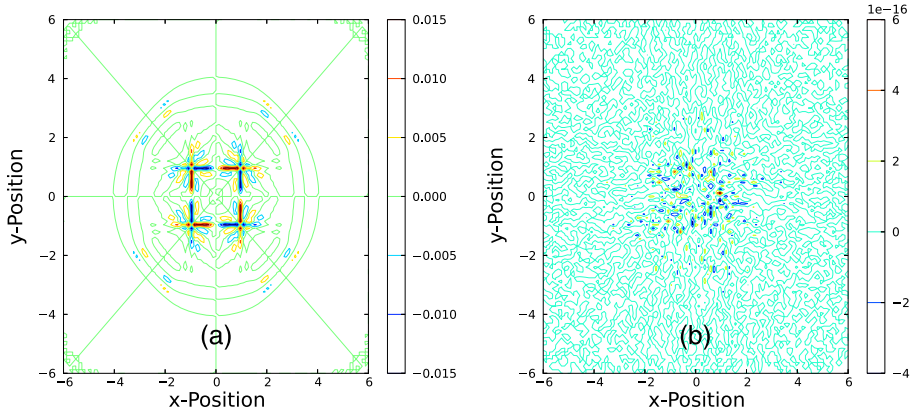

Figure 3. Compact vorticity contours predicted by LW (a) and RR (b) at $t = 3$. Computations were run with $\nu = 0.6$. The LW method generates spurious vorticity, but the RR method maintains zero vorticity to double precision.

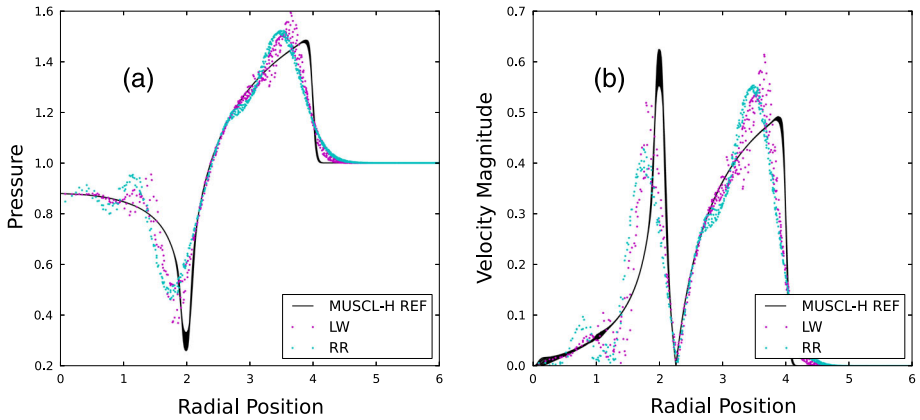

Figure 4. LW and RR comparison: Pressure (a) and velocity magnitude (b) profiles for the discontinuous test problem plotted at $t = 3$. Computations were run with $\nu = 0.6$.

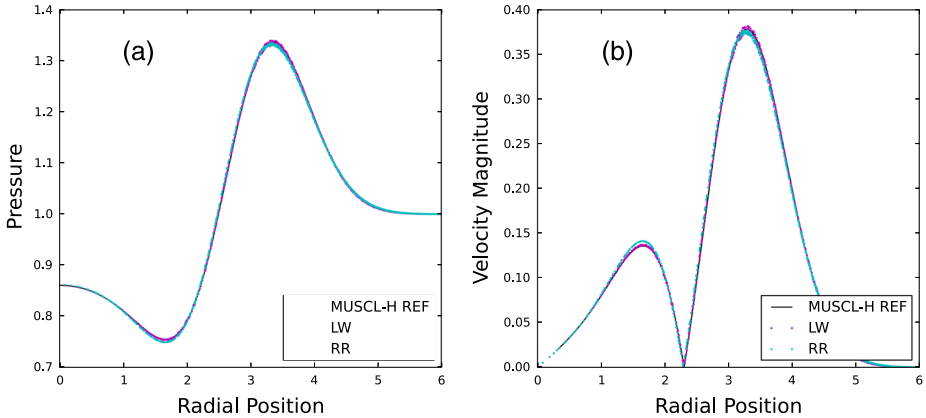

Figure 5. LW and RR comparison: Pressure (a) and velocity magnitude (b) profiles for the Gaussian test problem plotted at $t = 3$. Computations were run with $\nu = 0.6$.

DOI: 10.1002/fld

3.2. *Parameterization of the Lax–Wendroff family*

When using a nine point stencil in two spatial dimensions, there is considerable freedom in how a LW type scheme can be formulated. Here, we parameterize this family of schemes in the most general way possible. The LW scheme can be derived by writing the Taylor expansion of $\mathbf{U}$ in time

$$\mathbf{U}^{n+1} = \mathbf{U}^n + \Delta t \mathbf{U}_t^n + \frac{\Delta t^2}{2!}\mathbf{U}_{tt}^n + O\left(\Delta t^3\right)$$

and then using (1) to replace the first and second order time derivatives with spatial derivatives. Denoting the flux Jacobians by $\underline{A} = \partial\mathbf{F}/\partial\mathbf{U}$ and $\underline{B} = \partial\mathbf{G}/\partial\mathbf{U}$, we have

$$\frac{\mathbf{U}^{n+1} - \mathbf{U}^n}{\Delta t} = -\mathbf{F}_x - \mathbf{G}_y + \frac{\Delta t}{2}\left[\underline{A}\left(\mathbf{F}_{xx} + \mathbf{G}_{yx}\right) + \underline{B}\left(\mathbf{F}_{xy} + \mathbf{G}_{yy}\right)\right] + O\left(\Delta t^2\right). \tag{3}$$

The exact spatial derivatives in (3) must now be replaced with appropriate central difference approximations. These discretizations are not uniquely defined on the nine point stencil except in the case of the second order mixed partial derivative. The final approximations for $()_x$, $()_{xx}$, $()_y$, and $()_{yy}$ must be constrained so that x is treated equitably with y, and u with v. However, the weights assigned to the pressure derivatives need not be the same as those given to the velocities. Taken together, these guidelines result in four free parameters, $\alpha_1, \alpha_2, \phi_1$ and ϕ_2. The α weights were used for pressure derivatives, while the ϕ weights were used for velocity derivatives. The subscripts one and two represent whether the parameter applies to first or second order derivative approximations, respectively. An example parameterization for a second derivative is shown in Figure 6.

Writing the general form of the scheme as

$$\mathbf{U}^{n+1} = \mathbf{U}^n + \underline{T}\mathbf{U}^n \tag{4}$$

the parameterized evolution operator, $\underline{T}$, is given by

$$\underline{T} = \begin{bmatrix} \frac{\nu^2}{2}\left(\delta_x^2\left(1+\alpha_2\delta_y^2\right) + \delta_y^2\left(1+\alpha_2\delta_x^2\right)\right) & -\nu\mu_x\delta_x\left(1+\phi_1\delta_y^2\right) & -\nu\mu_y\delta_y\left(1+\phi_1\delta_x^2\right) \\ -\nu\mu_x\delta_x\left(1+\alpha_1\delta_y^2\right) & \frac{\nu^2}{2}\delta_x^2\left(1+\phi_2\delta_y^2\right) & \frac{\nu^2}{2}\mu_x\mu_y\delta_x\delta_y \\ -\nu\mu_y\delta_y\left(1+\alpha_1\delta_x^2\right) & \frac{\nu^2}{2}\mu_x\mu_y\delta_x\delta_y & \frac{\nu^2}{2}\delta_y^2\left(1+\phi_2\delta_x^2\right) \end{bmatrix}. \tag{5}$$

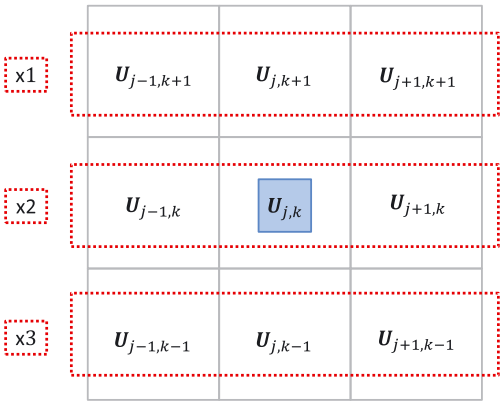

Figure 6. Example parameterization for the approximation of the second derivative of a generic state variable U with respect to x.

DOI: 10.1002/fld

The challenge is to determine the best choices for the four free parameters so as to find an optimal LW type method in two spatial dimensions using a nine point stencil. Of course, this has been attempted many times in the past. We will highlight a few examples. Lax and Wendroff extended their original one-dimensional method [18] to two spatial dimensions in [19]. The simplest scheme they proposed, and the one we take to be the 'original' two-dimensional LW method, did not use the corner points except in the case of the second order mixed partial derivative. They also suggested a method that included a dissipation term which is proportional to the fourth order mixed partial derivative ∂_{xxyy}. Strang constructed a multidimensional LW type method from the one-dimensional LW difference operators in [20]. Like the schemes proposed by Lax and Wendroff, the corner points were not used in the approximations for u_x, u_{xx}, u_y, or u_{yy}. However, Strang's scheme included terms that approximated both third and fourth order derivatives. This and other early work was summarized by Turkel [15] about a decade later. Gottlieb and Turkel [21] derived a modified LW method by considering the phase error. Another class of schemes, which are interesting due to the manner of derivation, have been developed by Lukáčová-Medvid'ová *et al.* [22] using their evolution Galerkin approach and the bicharacteristic form of the equations. We took a different path in analyzing the parameterized Lax–Wendroff family of schemes. A two-dimensional dispersion analysis was performed to show how the isotropy of the numerical dispersion relations depended upon the free parameters. This dependence was to be minimized. While considerable gains were realized earlier by enforcing vorticity preservation, we will begin by only considering the isotropy of the dispersion relations. Later, a connection between the two properties is made. All of the schemes discussed are described by special cases of (5).

3.3. Dispersion analysis

A two-dimensional von Neumann analysis was performed on the parameterized scheme. This exposed anisotropic terms in the numerical dispersion relationships and highlighted choices of parameters that would eliminate them. To begin the analysis, a two-dimensional von Neumann substitution of the form $u^n_{j,k} = g^n \exp[i\, r\, \theta_r]\mathbf{r} = g^n \exp[i\,(\theta_x\, j + \theta_y k)]\mathbf{r}$ was carried out with (4). Here, $i = \sqrt{-1}$. This substitution assumes plane (or line) wave solutions that have frequency θ_r in the direction ψ, which is measured from the positive x-axis. With some simplification, the equation reads

$$g\mathbf{r} = \mathbf{r} + \underline{T}\mathbf{r}.$$

After some manipulation and letting $\underline{I} + \underline{T} = \widehat{\underline{T}}$, the standard eigenvalue problem can be recovered

$$\widehat{\underline{T}}\mathbf{r} = g\mathbf{r}.$$

Here, g represents the eigenvalues of the matrix $\widehat{\underline{T}}$ and $\mathbf{r}$ represents the eigenvectors. For the problem at hand, $\widehat{\underline{T}}$ is a 3x3 matrix. The three resulting eigenvalues are interpreted as follows. One is real and relates to the stationary vorticity mode; it should be exactly unity. The other two eigenvalues, which are a complex conjugate pair, represent right and left going acoustic waves. The magnitude of the eigenvalues gives the amplification factors, while their arguments give the phase changes per time step. After computing the eigenvalues symbolically, they can be expanded with respect to the signal frequency θ_r. The resulting expressions are

$$\begin{aligned} g_1 = 1 &- \frac{\nu^2\theta_r^4}{32}(1-4\phi_2)\sin^2 2\psi \\ &+ \frac{\nu^2\theta_r^6}{768}\left[3(1-4\alpha_1)(1-4\phi_1)\sin^2 2\psi - 2(1-4\phi_2)\right]\sin^2 2\psi + O\left(\theta_r^8\right) \end{aligned} \tag{6}$$

$$\begin{aligned} g_{2,3} = 1 &\pm i\,\nu\theta_r - \frac{\nu^2\theta_r^2}{2} \mp i\,\frac{\nu\theta_r^3}{24}\left[4 - 2(1-3(\alpha_1+\phi_1))\left(1-2\sin^2 2\psi\right)\right] \\ &+ \frac{\nu^2\theta_r^4}{192}\left[8 + (1-12\phi_2-24\alpha_2)\sin^2 2\psi\right] + O\left(\theta_r^5\right). \end{aligned} \tag{7}$$

DOI: 10.1002/fld

It is immediately apparent that something special will happen to g_1 when any parameter is set equal to 1/4, which corresponds to evaluating the relevant term from vertex fluxes. For the RR scheme, all of the parameters take this value. To maximize isotropy, terms that depend on the wave orientation ψ should be eliminated. The potentially anisotropic fourth order term in (6) can be eliminated if $\phi_2 = 1/4$, so that g_1 becomes

$$g_1 = 1 - \frac{\nu^2\theta_r^6}{256}(1-4\alpha_1)(1-4\phi_1)\sin^2 2\psi + O\left(\theta_r^8\right). \tag{8}$$

The sixth order term can also be removed by choosing either $\alpha_1 = 1/4$ or $\phi_1 = 1/4$. [¶] By comparing the RR evolution operator with our parameterized evolution operator $\underline{T}$, one can deduce that setting $\alpha_1 = 1/4$ and $\phi_2 = 1/4$ will recover the vorticity preservation property. The choice of ϕ_2 is the same as was specified earlier from the dispersion analysis. In addition, the quandry about whether to set $\phi_1 = 1/4$ or $\alpha_1 = 1/4$ has been resolved. It is interesting, however, that either choice results in a real, isotropic eigenvalue provided $\phi_2 = 1/4$. The choice of $\alpha_1 = 1/4$ corresponds to a family of schemes that exactly preserve compact vorticity. The choice of $\phi_1 = 1/4$ corresponds to a family of schemes that can exactly preserve physically correct steady solutions. For the sake of brevity, we will leave further discussion about these aspects of the Lax–Wendroff evolution matrix to a different paper.

We have now demonstrated a concrete link between vorticity control and isotropy. The two unique choices of α_1 and ϕ_2 that guarantee vorticity preservation also make the g_1 eigenvalue isotropic. However, there is still complete freedom in choosing α_2 and ϕ_1. We refer to this family of schemes as vorticity preserving Lax–Wendroff (VPLW). The eigenvalue expansions now read

$$g_1 = 1 \tag{9}$$

$$\begin{aligned} g_{2,3} = 1 \pm i\nu\theta_r - \frac{\nu^2\theta_r^2}{2} \mp i\frac{\nu\theta_r^3}{48}\left[8-(1-12\phi_1)\left(1-2\sin^2 2\psi\right)\right] \\ + \frac{\nu^2\theta_r^4}{96}\left[4-(1+12\alpha_2)\sin^2 2\psi + O\left(\theta_r^5\right).\right] \end{aligned} \tag{10}$$

Inspection of (10) shows that the next two anisotropic terms could be eliminated by choosing $\phi_1 = 1/12$ and $\alpha_2 = -1/12$. The resulting scheme, denoted as VPLW1, is maximally isotropic. Results from this scheme are presented in Figure 7. The isotropy of the solution is improved to the point that it exceeds that of the reference solution. While this is impressive, numerical experiments showed that the stability of the scheme was reduced, perhaps because of the negative weight. The RR scheme is maximally stable up to a Courant number of one, while the VPLW1 method was observed to go unstable around $\nu = 0.7$. Because maximal stability was desired, the negative weight was discarded and a suitable positive replacement was sought for α_2.

The α_2 parameter controls the discretization of the second order terms in the pressure update equation, which approximate the Laplacian of the pressure. An isotropic spatial discretization for the scalar wave equation was proposed by Vichnevetsky and Bowles in [23]. It is obtained here by taking $\alpha_2 = 1/8$ and leads to

$$\nabla^2() \approx \left(\delta_x^2 + \delta_y^2 + \frac{1}{4}\delta_x^2\delta_y^2\right)()/h^2 = \nabla^2() + \frac{h^2}{12}\nabla^4() + O\left(h^4\right).$$

This was shown to be the most isotropic way to represent the Laplacian on nine points in [24]. [‖]

[¶]In fact with these choices, g_1 becomes exactly unity, because $\det(\underline{T})$ can be shown to vanish.

[‖]However, taking $\alpha_1 = \phi_2 = 1/4$ is not the most isotropic way to evaluate the first derivatives. Instead, it is the choice that gives overall the most isotropic behavior. That is why we asserted earlier that the Lax–Wendroff family can only be optimized with a specific problem in mind.

DOI: 10.1002/fld

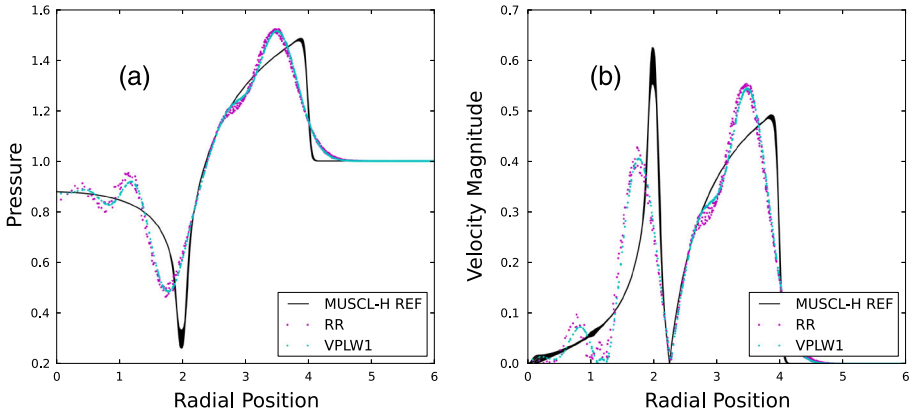

Figure 7. RR and VPLW1 comparison: Pressure (a) and velocity magnitude (b) profiles for the discontinuous test problem plotted at $t = 3$. Computations were run with $\nu = 0.6$.

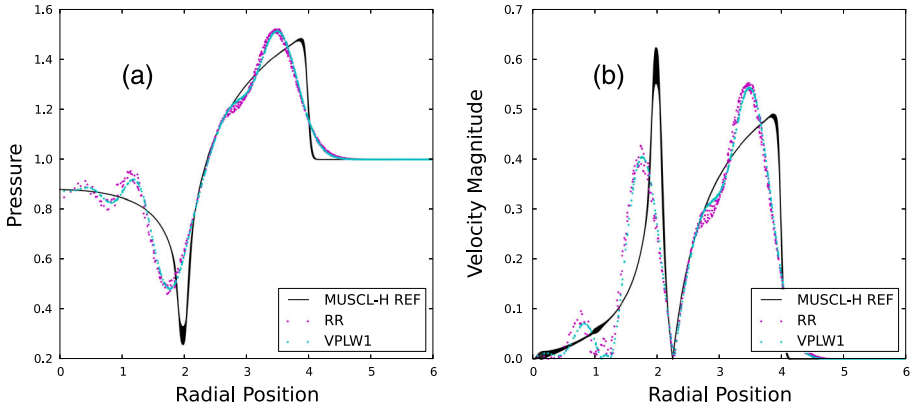

Figure 8. RR and VPLW2 comparison: Pressure (a) and velocity magnitude (b) profiles for the discontinuous test problem plotted at $t = 3$. Computations were run with $\nu = 0.6$.

The scheme that is defined by $\phi_1 = 1/12$ and $\alpha_2 = 1/8$ is denoted as VPLW2. Inspection of the results shown in Figure 8 shows that the isotropy of the VPLW2 scheme is still improved over RR. In addition, numerical experiments have indicated that the VPLW2 scheme is stable up to a Courant number of one.

Due to the favorable combination of isotropy and stability, we take VPLW2 as our preferred choice and write it in finite volume (FV) form. Denoting vertex fluxes by $\hat{()}$ and face fluxes by $\tilde{()}$, the VPFV2 scheme is written as

$$\mathbf{U}^{n+1} = \mathbf{U}^n - \frac{\Delta t}{h}\left(\mu_y\delta_x\hat{\mathbf{F}} + \mu_x\delta_y\hat{\mathbf{G}} + \delta_x\tilde{\mathbf{F}} + \delta_y\tilde{\mathbf{G}}\right) \tag{11}$$

where, taking $q = \nu^2$, the fluxes are defined by

$$\hat{\mathbf{F}} = \begin{pmatrix} \frac{1}{3}\mu_x\mu_y au - \frac{qh}{4\Delta t}\mu_y\delta_x p \\ \mu_x\mu_y ap - \frac{qh}{2\Delta t}\left(\mu_y\delta_x u + \mu_x\delta_y v\right) \\ 0 \end{pmatrix}$$

$$\hat{\mathbf{G}} = \begin{pmatrix} \frac{1}{3}\mu_x\mu_y av - \frac{qh}{4\Delta t}\mu_x\delta_y p \\ 0 \\ \mu_x\mu_y ap - \frac{qh}{2\Delta t}(\mu_y\delta_x u + \mu_x\delta_y v) \end{pmatrix}$$

DOI: 10.1002/fld

$$\tilde{\mathbf{F}} = \begin{pmatrix} \frac{2}{3}\mu_x a u - \frac{qh}{4\Delta t}\delta_x p \\ 0 \\ 0 \end{pmatrix} \qquad \tilde{\mathbf{G}} = \begin{pmatrix} \frac{2}{3}\mu_y a v - \frac{qh}{4\Delta t}\delta_y p \\ 0 \\ 0 \end{pmatrix}. \tag{12}$$

Note that altering the pressure update equation has led to pressure fluxes being stored at both vertices and faces. Although this adds some expense, we feel that the cost increases are justified by the increase in isotropy. Despite a portion of the flux being located at face centers, the vertex fluxes still define a unique velocity that could be used to move the mesh in a Lagrangian algorithm.

4. CRISIS II: SPURIOUS EXTREMA

4.1. General considerations

As a member of the Lax–Wendroff family, the VPFV2 scheme is second order accurate in space and time. This means a nonlinear limiting process must be used in order to prevent spurious extrema from entering the solution. When setting out to design a limiter, three fundamental questions arise immediately:

1. What quantities should the limiter act on?
2. How should 'monotonicity' be defined for multidimensional, nonscalar problems?
3. How should the limiting mechanism be designed?

4.1.1. Choosing quantities to limit on. There are many possible answers to the first question and each offers some advantages. For example, conserved variables are easily accessed when dealing with finite volume algorithms and primitive variables can be advantageous when seeking to enforce positivity for pressure, energy, or density. In one dimension, characteristic variables are often favored (see, e.g., [25]). It is proposed here to use what we refer to as 'driver quantities'. These quantities drive the time evolution of the vertex fluxes. Using the Lax–Wendroff type procedure, the acoustic fluxes can be expanded through first order as

$$(a_0\mathbf{V})^{n+1} = (a_0\mathbf{V})^n - \frac{a_0 k}{2}\nabla(a_0 p)^n \qquad (a_0 p)^{n+1} = (a_0 p)^n - \frac{a_0 k}{2}\nabla\cdot(a_0\mathbf{V})^n. \tag{13}$$

Denoting driver quantities as β, we set $\beta = \nabla\cdot\mathbf{V}$ for the flux pressure and $\beta = \nabla p$ for the flux velocity. Note that these driver quantities have the advantage of being rotationally invariant. They should, at least in principle, be independent of the mesh, and whatever the limiting process is, it should not change this invariance. In our case care has been taken to make the base schemes as isotropic as possible. If the direction of the pressure gradient is accepted, then all that remains to be considered is the magnitude. As a result, we limit based only on the magnitude of the pressure gradient, $\beta = |\nabla p|$, for the flux velocity.

4.1.2. Defining monotonicity. The question of 'how much' to limit is made more difficult by the fact that there are no rigorous bounds on the solution to the multidimensional acoustic problem. For one-dimensional linear problems, the characteristic variables obey a maximum principle, but in higher dimensions, the strongest condition available is that the 'energy' $p^2 + \mathbf{u}\cdot\mathbf{u}$ is conserved and therefore bounded in an integral sense [26]. This invalidates the usual limiting procedures used in Riemann solver-based methods that place bounds on one-dimensional gradients and has inclined us toward the more qualitative form of limiting associated with the FCT concept originally proposed by Boris and Book [27].

4.1.3. Designing the limiting mechanism. The FCT framework uses a 'cautious' first order scheme to advect and diffuse the data through one time step. Provided the first order scheme has sufficient diffusion, no spurious extrema will be admitted. As a result, the new solution given by the cautious scheme can be taken to define what a well-behaved, or 'monotone', solution looks like. The job of the flux limiter is then to ensure that no new features appear during the antidiffusion step. Similarly,

DOI: 10.1002/fld

we plan to use an appropriate first order scheme to dynamically define the concept of a well-behaved solution. Liu and Lax have developed schemes that are positive in the sense of the solution energy norm [28]. However, their derivations did not try to build in rotational invariance and relied on traditional one-dimensional limiting statements. So, we have adopted a different approach, but hope to make use of some of their ideas.

The ideal first order base scheme would

- introduce the minimum amount of diffusion needed to prevent spurious extrema;
- introduce minimal phase error; and
- be isotropic and vorticity preserving.

A starting point in the quest for a cautious scheme might be to seek analogs of the one-parameter family of q-schemes defined on a three-point stencil for one-dimensional linear advection. The family is written as

$$u_j^{n+1} = u_j^n - \frac{\nu}{2}\left(u_{j+1}^n - u_{j-1}^n\right) + \frac{q}{2}\left(u_{j-1}^n - 2u_j^n + u_{j+1}^n\right) \tag{14}$$

or, alternatively, in terms of an interface flux

$$f_{j+1/2} = \frac{a}{2}\left(u_j + u_{j+1} - \frac{q}{\nu}(u_{j+1} - u_j)\right). \tag{15}$$

Note that in the expression for the flux the factor q is applied to the estimated gradient u_x, which is the driver quantity in this case. If q is taken to be a global constant, optimal members of the family with respect to diffusion and phase error are known (see, e.g., [29]). The first order upwind (FUP) scheme has the minimal amount of diffusion needed to guarantee monotonicity and is obtained by setting $q = |\nu|$. The low phase error (LPE) scheme introduces minimal phase error [30] and requires $q = 1/3 + 2\nu^2/3$. Also recall that the Lax–Wendroff method is recovered if $q = \nu^2$. Schemes with various properties are recovered by tuning a single parameter, which is in fact the only parameter available on a three-point stencil. The limiting strategy applied here involves choosing a value for q that yields a high order scheme, for which the only possibility in one-dimension is $q_H = \nu^2$, and some low order q_L, and then imposing a limiter on the antidiffusive part of the driver

$$\beta_{AD} = \frac{q_H - q_L}{\nu}(u_{j+1} - u_j)$$

The family of two-dimensional schemes on a nine-point stencil is much richer, and we have only begun to explore it. Instead of a single dissipative term to be tuned there are 12, even after taking symmetry into account. This richness is hard to analyze but seems to be needed because simple analogs of the one-dimensional treatment have been found to fail. For example, the simplest scheme that would recover first order upwinding in one dimension is very oscillatory when a wave travels at 45° to the mesh.

Here, preliminary results are shown from a scheme that did make use of only a single parameter; it uses the VPLW2 evolution operator and sets $q = 0.8\nu + 0.2\nu^2$. This value for q was obtained through extensive numerical experiments and the resulting scheme is designated VPFV2-O1. Results that give an example of the problems with the RR-FUP analog and the subsequent improvements realized with the VPFV2-O1 scheme are presented in Figure 9.

Provisionally, we proceed with this choice for the cautious scheme while suspecting that it can be greatly improved upon.

4.2. A vorticity preserving flux limiter

As pointed out by Morton and Roe [10], vorticity preservation is not harmed as long as the limiting for the velocity equations is done on the *nodal* fluxes. While this requirement does not extend to the pressure update equation, it seems logical to be consistent and focus on driver quantities located at the nodes for now. Conveniently, the isotropic base scheme already computes the desired nodal quantities.

DOI: 10.1002/fld

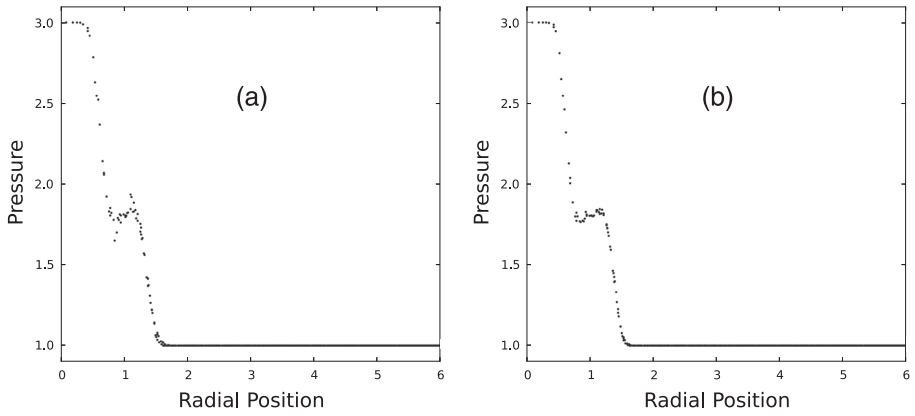

Figure 9. Comparison of the RR-FUP and VPFV2-O1 methods on the discontinuous test problem at $t = 0.288$. Computations were run with $\nu = 0.8$.

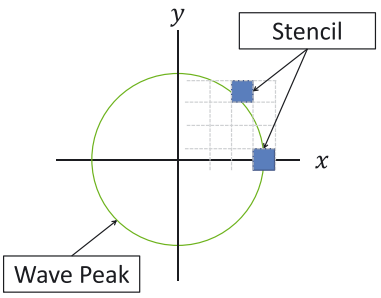

Figure 10. Anisotropy can be introduced if a limiter looks to spatial neighbors for information during the limiting process. Here, the orientation of the stencil to the wave peak is a function of position, and thus, calculations that naively use this information will likely yield anisotropic results.

The limiting philosophy that we employ is based on that of FCT. The original FCT scheme and flux limiter published by Boris and Book were derived for one dimension and prone to clipping. Their first extension to higher dimensions relied on the same one-dimensional arguments [31]. Zalesak introduced the first multidimensional flux limiter for use in a FCT context and also made contributions to reduce clipping [32]. These traditional flux limiters require *a priori* bounds to be placed on the solution in each cell at each time step. The bounds are specified based on the values of spatial neighbors. There are two potential problems with this approach. First, as already discussed, there is no way to properly calculate what the bounds should be. Second, using spatial neighbors to define the bounds is likely to introduce anisotropy into the scheme. Take for example the case of a circular wave peak traveling through two-dimensional space as shown in Figure 10. If the wave is resolved on a square mesh, the orientation of the stencil relative to the wave peak is a function of position. Assuming the limiter only has access to the information contained within the stencil, the allowable bounds calculated for the wave peak will also be a function of position. The same issue can also be made apparent by comparing the bounds the limiter would calculate for a plane wave aligned with the grid and the same wave traveling at 45° to the grid. A different approach that avoids these problems will now be proposed.

We have already identified the rotationally invariant driver quantities, β, that should be used. Now, three independent estimates of the drivers are calculated: one estimate is obtained from the current data (β^n), another from a provisional solution obtained with the cautious scheme (β^*_C), and the last from a provisional solution obtained with the accurate scheme (β^*_A). This is similar to the MUSCL approach where one obtains estimates of the gradient from different stencils. In general, the limiter should only accept the accurate driver estimate (and therefore the full antidiffusive flux) if it is within some tolerance of the cautious one. Otherwise, the three estimates should be combined

DOI: 10.1002/fld

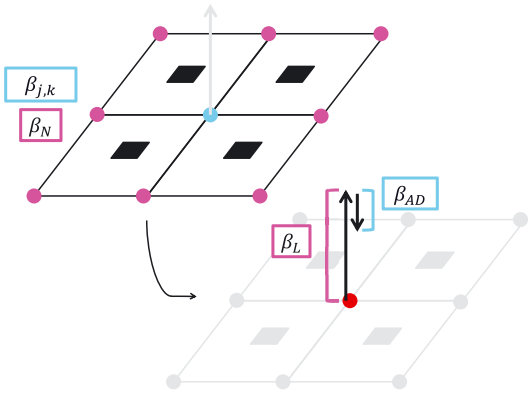

Figure 11. A graphical comparison of the traditional limiting methodology and the proposed flux limiter. The neighboring information needed to compute the driver quantity decomposition is completely handled by the isotropic base schemes. As a result, the limiter itself can be viewed as zero dimensional with respect to space. This construction guarantees that the limiter cannot be any less isotropic than the base schemes.

in a way that favors the cautious choice. Symbolically,

$$\beta^{n+1} = \text{fn}(\beta^n, \beta_C^*, \beta_A^*). \tag{16}$$

There is a kind of spatial limiting involved here because the drivers based on the provisional estimates at $n+1$ use a larger stencil than those based on the data at n. Drivers based on these different stencils are being compared, but only on the basis of the temporal changes that they induce. There are a large number of possible variations on this procedure, and we have only just begun to explore them.

In this paper, we proceed by subtracting the two provisional driver estimates to yield a quantity that is analogous to an antidiffusive flux: $\beta_{AD}^* = \beta_A^* - \beta_C^*$. Observe that this definition will change if we choose a different cautious (or accurate) scheme and that it is analogous to the flux decomposition of FCT. A limiting statement can now be formulated that restricts the amount by which the antidiffusive driver is allowed to change the cautious first order estimate. Written in terms of a limiting coefficient, χ, that will multiply the antidiffusive flux we write

$$\chi|\beta_{AD}^*| \leqslant f(\phi, \nu)|\beta_C^*|. \tag{17}$$

The reader will note the appearance of an indicator quantity ϕ and function f in (17). Both of these have the capability to influence the phase and amplitude performance of the final scheme. The simplest possible way to procede would be to discard the indicator quantity and set $f = \text{fn}(\nu)$. This forces a conservative approach because f is not able to assess the difficulty of the local data. Despite this seemingly naive approach, the current implementation uses $f = 0.0125\nu$, and the numerical results are very encouraging. It seems reasonable that the limiting performance could be improved further by introducing an indicator quantity and an obvious choice is β^n. This is one area of future work. It should be stressed, though, that there are many other ways in which the limiting framework described in (16) could be implemented. However, we are encouraged by the fact that merely plausible choices already give results that are very competitive in resolution with the more usual approaches while maintaining better symmetry.

To summarize, the new vorticity preserving flux limiter acts on forward temporal changes of the vertex fluxes. The neighboring information required to compute the vertex-centered driver quantities is handled exclusively by the isotropic base schemes. As a result, the limiter itself deals only with the point wise time evolution and could be described as zero dimensional with respect to space. In addition, a cautious first order scheme and the function f have been used to eliminate the need to specify *a priori* bounds on the solution. The end result is a local, multidimensional limiter that is efficient and easy to code. An illustration that compares this approach with the traditional one is included in Figure 11.

DOI: 10.1002/fld

4.3. Numerical recipe and implementation notes

The final method is an FCT implementation that uses the VPFV2 scheme as the high order ingredient, the VPFV2-O1 scheme as the low order ingredient, and the flux limiter described in the previous section. This will be referred to as the VPFCT scheme. Two limiting coefficients for vertex fluxes are calculated independently: one for the pressure update and one for the velocity updates. Additionally, two limiting coefficients were needed to limit the face fluxes in the pressure update equation. These were calculated by simply averaging the values of the adjacent nodal coefficients.

The VPFCT scheme advances the solution one time step via the following process:

1. Calculate a first order provisional solution:

$$\boldsymbol{U}_{\boldsymbol{C}}^{*} = \boldsymbol{U}^{\boldsymbol{n}} + \tfrac{\Delta t}{h}\left[\mu_y\delta_x\hat{\boldsymbol{F}}_{\boldsymbol{C}} + \mu_x\delta_y\hat{\boldsymbol{G}}_{\boldsymbol{C}} + \delta_x\tilde{\boldsymbol{F}}_{\boldsymbol{C}} + \delta_y\tilde{\boldsymbol{G}}_{\boldsymbol{C}}\right]$$

2. Calculate a second order provisional solution:

$$\boldsymbol{U}_{\boldsymbol{A}}^{*} = \boldsymbol{U}^{\boldsymbol{n}} + \tfrac{\Delta t}{h}\left[\mu_y\delta_x\hat{\boldsymbol{F}}_{\boldsymbol{A}} + \mu_x\delta_y\hat{\boldsymbol{G}}_{\boldsymbol{A}} + \delta_x\tilde{\boldsymbol{F}}_{\boldsymbol{A}} + \delta_y\tilde{\boldsymbol{G}}_{\boldsymbol{A}}\right]$$

3. Calculate limiting coefficients and assemble the limiting vectors $\hat{\boldsymbol{\chi}}_{\boldsymbol{F}}$, $\hat{\boldsymbol{\chi}}_{\boldsymbol{G}}$, $\tilde{\boldsymbol{\chi}}_{\boldsymbol{F}}$, and $\tilde{\boldsymbol{\chi}}_{\boldsymbol{G}}$. The approximations for the driver quantities are those already contained in the fluxes of the base scheme:

$$\hat{\chi}_p|\nabla p^*_{AD}| \leqslant f_p(\nu)|\nabla p^*_C| \qquad \hat{\chi}_V\left|\left(\nabla\cdot\mathbf{V}^*_{AD}\right)\right| \leqslant f_V(\nu)\left|\left(\nabla\cdot\mathbf{V}^*_C\right)\right|$$

$$|\nabla p| \approx \sqrt{\left[\mu_y\delta_x p/h\right]^2 + \left[\mu_x\delta_y p/h\right]^2} \qquad |\nabla\cdot\mathbf{V}| \approx \left|\left(\mu_y\delta_x u + \mu_x\delta_y v\right)/h\right|$$

$$\hat{\boldsymbol{\chi}}_F = \begin{pmatrix}\hat{\chi}_p\\ \hat{\chi}_V\\ 0\end{pmatrix} \qquad \hat{\boldsymbol{\chi}}_G = \begin{pmatrix}\hat{\chi}_p\\ 0\\ \hat{\chi}_V\end{pmatrix} \qquad \tilde{\boldsymbol{\chi}}_F = \begin{pmatrix}\tilde{\chi}_{px}\\ 0\\ 0\end{pmatrix} \qquad \tilde{\boldsymbol{\chi}}_G = \begin{pmatrix}\tilde{\chi}_{py}\\ 0\\ 0\end{pmatrix}$$

4. Calculate the limited high order solution:

$$\boldsymbol{U}^{\boldsymbol{n+1}} = \boldsymbol{U}_{\boldsymbol{C}}^{*} + \tfrac{\Delta t}{h}\left[\mu_y\delta_x\hat{\boldsymbol{\chi}}_{\boldsymbol{F}}\hat{\boldsymbol{F}}_{\boldsymbol{AD}} + \mu_x\delta_y\hat{\boldsymbol{\chi}}_{\boldsymbol{G}}\hat{\boldsymbol{G}}_{\boldsymbol{AD}} + \delta_x\tilde{\boldsymbol{\chi}}_{\boldsymbol{F}}\tilde{\boldsymbol{F}}_{\boldsymbol{AD}} + \delta_y\tilde{\boldsymbol{\chi}}_{\boldsymbol{G}}\tilde{\boldsymbol{G}}_{\boldsymbol{AD}}\right]$$

The results presented in the next section were obtained by setting $f_p = f_V = 0.0125\nu$ for both the pressure and velocity limiting statements. This function was determined empirically.

At first glance the proposed scheme may appear to be expensive due to the computation of a first order step, an unlimited second order step, and the final update. However, straightforward coding can minimize the extra computations needed because the first and second order methods are identical except for a modified q term. Of course, the fact that the scheme is stable up to $\nu = 1$ is also advantageous.

5. NUMERICAL RESULTS

Solutions to the discontinuous test problem were computed with the VPFV2-O1, unlimited VPFV2, and VPFCT algorithms and plotted on the same set of axes in Figure 12. Results are shown on two different meshes: 100×100 and 600×600. Comparing the solutions obtained with the VPFCT ingredients to the final product helps illustrate how the cautious scheme, accurate scheme, and temporal flux limiter work together to produce a solution that is free from spurious features. It is observed that the limiter is able to identify the problem areas in the high order solution and correct them while incurring minimal damage to the physical waves. On the coarse grid, the limiter is able to use the cautious scheme to not only remove the spurious features from the VPFV2 scheme but also reduce the amount of mesh imprinting in some regions.

The performance of the final VPFCT scheme will now be compared to an unsplit MUSCL-Hancock method that uses a harmonic slope limiter. The MUSCL-Hancock scheme is only stable

DOI: 10.1002/fld

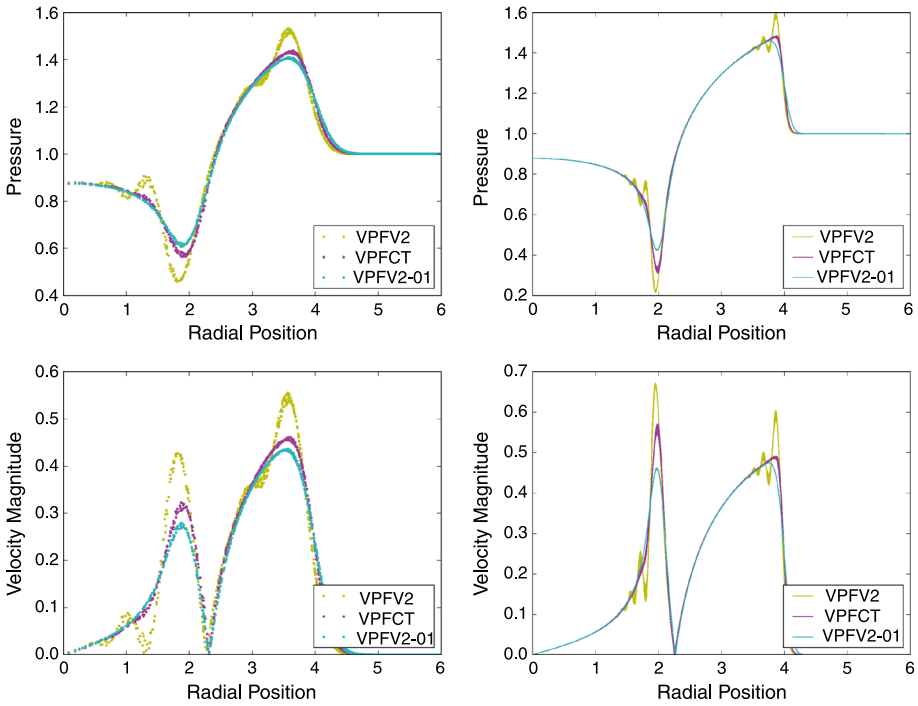

Figure 12. Comparison of the VPFV2-O1, unlimited VPFV2, and VPFCT schemes for the discontinuous pressure problem on two different meshes ($\nu = 0.8$, $t = 3$): (a) Pressure, 100×100 mesh; (b) Pressure, 600×600 mesh; (c) Velocity magnitude, 100×100 mesh; (d) Velocity magnitude, 600×600 mesh.

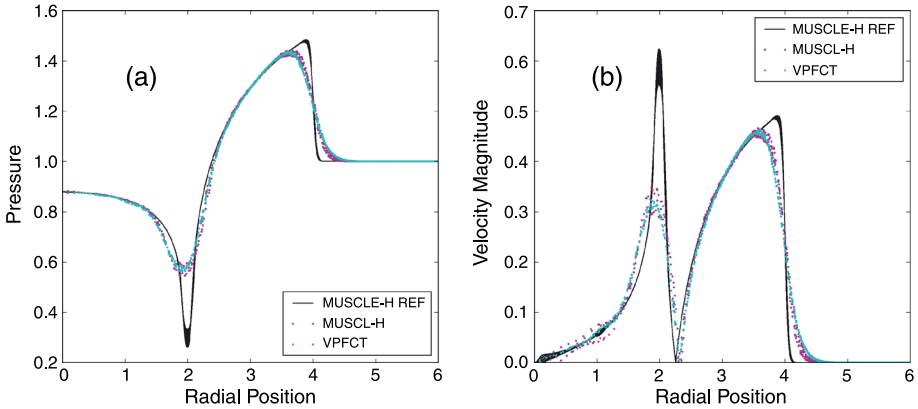

Figure 13. MUSCL-H ($\nu = 0.4$) and VPFCT ($\nu = 0.8$) comparison: Pressure (a) and velocity magnitude (b) profiles for the discontinuous test problem plotted at $t = 3$.

up to $\nu = 0.5$. Because the accuracy of the phase and amplitude relations for both schemes depend on the Courant number, comparisons will be conducted at Courant numbers that correspond to the same percentage of the respective theoretical maximums. (e.g., $\nu = 0.4$ for MUSCL-H and $\nu = 0.8$ for VPFCT correspond to 0.8 of the maximum allowable values)

Results are presented in Figure 13 for the discontinuous test problem that has been used throughout this paper. Here, we see that the VPFCT scheme has comparable phase and amplitude performance to MUSCL-H, but superior isotropy. The improvement in isotropy is particulary evident in the velocity magnitude plot.

The ability of the VPFCT scheme to preserve physical vorticity will be demonstrated with a new test problem that combines a steady vortical flow with the two-dimensional unsteady interaction of four planar pressure waves. The initial velocity data form a modified combination vortex in which

DOI: 10.1002/fld

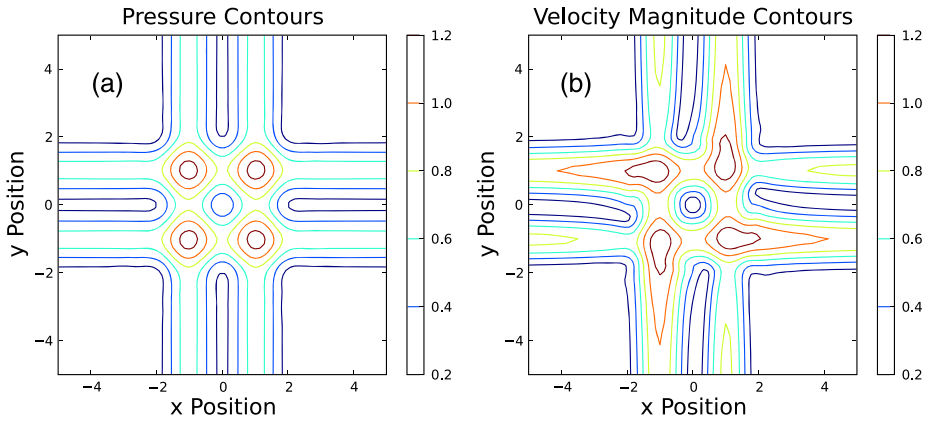

Figure 14. Intermediate results from a computation in which four plane waves interact with a steady, rotational velocity field (300 × 300 mesh, $t = 0.9$, $\nu = 0.8$) demonstrate the complexity of the transient flow. (a) Pressure contours computed with the VPFCT method; (b) Velocity magnitude contours computed with the VPFCT method.

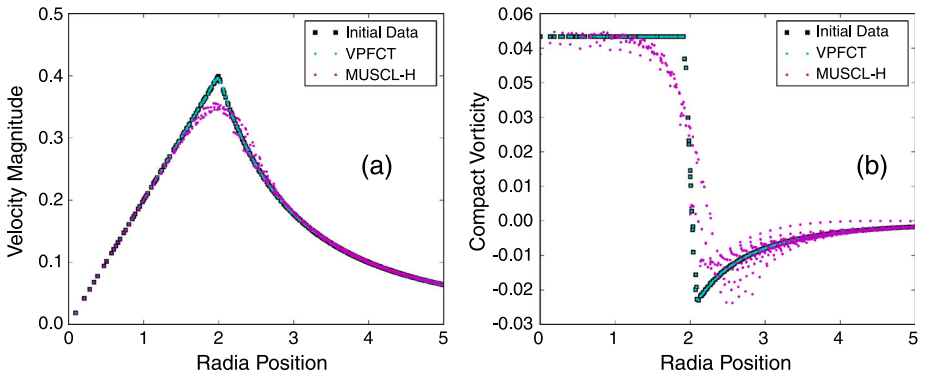

Figure 15. Final results from a computation in which four plane waves interact with a steady, rotational velocity field (300 × 300 mesh). (a) Comparison of the radial velocity magnitude profiles obtained with the VPFCT method ($\nu = 0.8$) and the MUSCL-H method ($\nu = 0.4$) at $t = 2$; (b) Comparison of the radial vorticity profiles obtained with the VPFCT method ($\nu = 0.8$) and the MUSCL-H method ($\nu = 0.4$) at $t = 2$.

the core is prescribed as the usual solid body rotation, but the potential vortex region is replaced with a tangential velocity field that decays with the square of the radial position, r. This makes the problem more interesting by introducing additional vorticity. The divergence of the velocity field is zero, and therefore, the data represent a steady solution if a uniform pressure field is specified. A series of plane wave disturbances centered at $x = -10$, $x = 10$, $y = -10$, and $y = 10$ with magnitude two were then introduced. Specifically, the initial conditions were defined on the domain $x \in [-20, 20]$ and $y \in [-20, 20]$ as

$$u(x, y, 0) = -\frac{y}{5} \qquad v(x, y, 0) = \frac{x}{5} \qquad \text{if } r \leqslant 2$$

$$u(x, y, 0) = -\frac{16y}{10(x^2 + y^2)^{3/2}} \qquad v(x, y, 0) = \frac{16x}{10(x^2 + y^2)^{3/2}} \qquad \text{if } r > 2$$

$$p(x, y, 0) = 2 \text{ if } x, y \in (-10.5, -9.5) \text{ or } x, y \in (9.5, 10.5), \text{ otherwise } p(x, y, 0) = 1 \quad a_0 = 10.$$

The plane waves split and part of each travels toward the origin. These waves influence the velocity field as they travel. Figure 14 shows contours of the pressure and velocity magnitude at $t = 0.9$ to demonstrate the complexity of the transient flow. However, at $t = 2$, the left and right going wave pairs in each direction have passed through each other and arrive at the locations of the initial disturbances. At this time, the velocity field in the inner region should have returned to the initial

DOI: 10.1002/fld

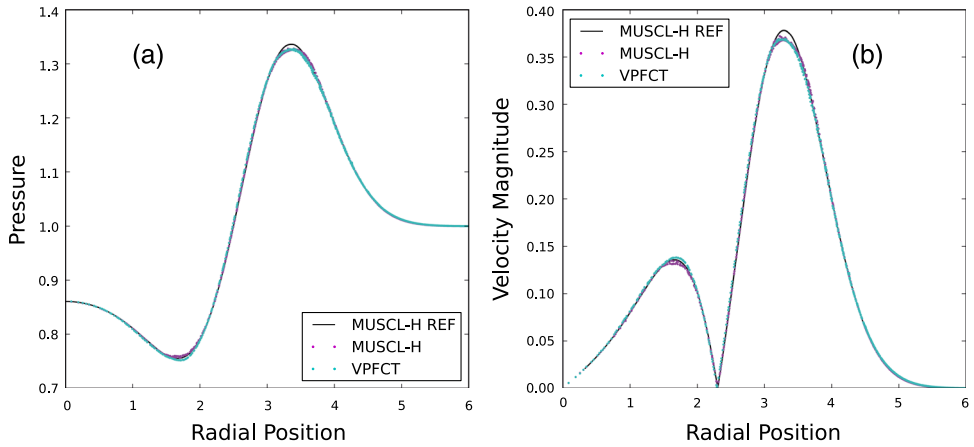

Figure 16. MUSCL-H ($\nu = 0.4$) and VPFCT ($\nu = 0.8$) comparison: Pressure (a) and velocity magnitude (b) profiles for the smooth Gaussian test problem plotted at $t = 3$.

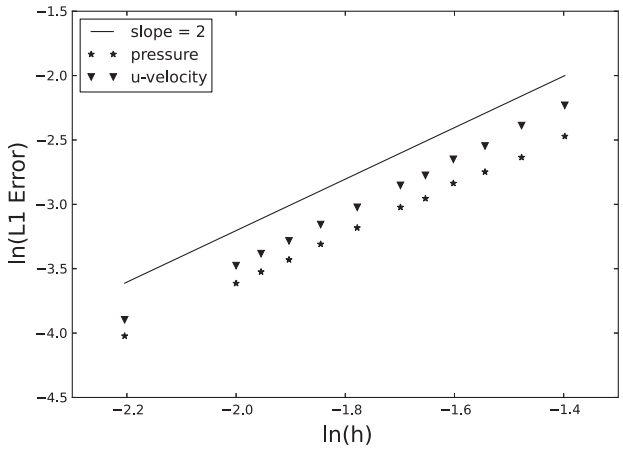

Figure 17. Convergence results for the VPFCT scheme on a smooth test problem. The Courant number for all runs was 0.8 and the meshes ranged from 50×50 to 320×320. The $L1$ errors were computed at $t = 0.375$. Both the convergence of pressure and u-velocity is shown.

state. Figure 15 compares the final velocity magnitude and vorticity fields obtained from the VPFCT algorithm and the MUSCL-H algorithm in a 10×10 square centered on the origin. The VPFCT algorithm is able to maintain the amplitude of the steady velocity solution with good accuracy and the radial symmetry of the solution is left intact. As expected, the vorticity field is exactly preserved. In contrast, the MUSCL-H scheme is not able to maintain the steady velocity solution or the vorticity solution and the radial symmetry of the problem is severely damaged.

Results from the smooth test problem used previously are shown in Figure 16. Clipping was not large and was on par with the harmonic slope limiter used by the MUSCL-H method. Further reducing clipping for smooth data is an area of ongoing work. Convergence results are presented in Figure 17 that show nearly optimal performance for smooth data, despite the limiter being applied. The plots were generated with a test problem taken from [22] in which a smooth periodic pressure distribution is applied to a fluid at rest. The initial conditions were defined on the domain $x \in [-1, 1]$ and $y \in [-1, 1]$ and set to

$$p(x, y, 0) = -\frac{1}{a_0}(\sin 2\pi x + \cos 2\pi y) \qquad u(x, y, 0) = v(x, y, 0) = 0 \qquad a_0 = 1.$$

DOI: 10.1002/fld

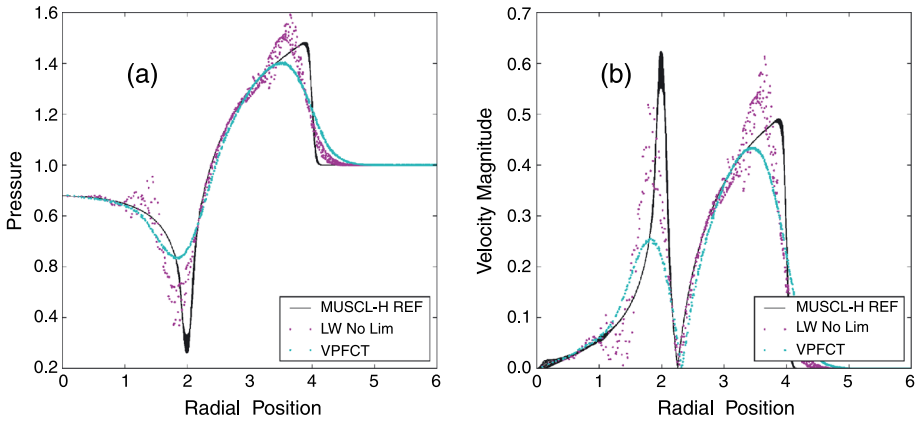

Figure 18. LW ($\nu = 0.6$) and VPFCT ($\nu = 0.6$) comparison: Pressure (a) and velocity magnitude (b) profiles for the discontinuous test problem plotted at $t = 3$.

The exact solution is then

$$p(x, y, t) = -\frac{1}{a_0} \cos 2\pi a_0 t (\sin 2\pi x + \cos 2\pi y)$$

$$u(x, y, t) = -\frac{1}{a_0} \sin 2\pi a_0 t \cos 2\pi x \qquad v(x, y, t) = -\frac{1}{a_0} \sin 2\pi a_0 t \cos 2\pi y.$$

Finally, this section is concluded with a plot that compares the original LW and VPFCT methods for the discontinuous test problem. See Figure 18. The VPFCT method uses the same stencil as the LW method and, in fact, is built using members of the same family of schemes. Despite these facts, its performance is dramatically improved. The vorticity preservation property, isotropic dispersion relations, and multidimensional flux limiter lead to an algorithm that makes better use of the available information.

6. CONCLUSIONS AND FUTURE WORK

A new vorticity preserving flux-corrected transport (VPFCT) scheme for the acoustic equations has been presented. Its derivation was motivated by the desire to reduce mesh imprinting and develop a multidimensional limiter that does not place *a priori* bounds on the solution. First, a comparison of numerical results obtained from the LW method and the vorticity preserving RR method were presented to show that vorticity control can reduce mesh imprinting. Analysis of the parameterized LW family was used to develop a concrete link between spurious vorticity generation and solution anisotropy (i.e., mesh imprinting). This involved comparing the results of a dispersion analysis to the constraints on free parameters imposed by vorticity preservation. The VPFV2 method resulted from this analysis and produced results that are superior to the rotated Richtmyer method. Next, a well-behaved first order scheme, VPFV2-O1, was obtained for use as the low order scheme in an FCT implementation. Finally, a multidimensional flux limiter was presented. The new limiter does not introduce isotropy into the solution, preserves vorticity, and acts on temporal changes in the driver quantities at vertices. At large Courant numbers, the final VPFCT scheme was shown to have comparable phase and amplitude performance to an unsplit MUSCL-H algorithm while suffering from less mesh imprinting. Furthermore, the VPFCT algorithm was shown to maintain physical vorticity when it is present. Near optimal convergence was demonstrated for the VPFCT scheme on a smooth test problem.

Areas of future work are planned. We have already begun to use this analysis as the foundation for a new Lagrangian hydrocode and the results are encouraging. Perhaps, however, there is still useful work to be done at the present, acoustic level. Further investigation of first order schemes that are well behaved and isotropic will be done. The simple implementation of the limiter presented here

DOI: 10.1002/fld

that sets $f = 0.0125\nu$ resulted in slight clipping. Ways to reduce this will be sought by using a local indicator of the flow complexity or different limiting statements. Third order implementations of the VPFCT method have been done in order to assess the resulting improvements to solution quality. A major goal here is to improve the phase error of the scheme, especially at low Courant numbers and for mid to high frequency data. A paper which takes a deeper look at the new limiter and explores the link between the limiter and third order accuracy is planned. Finally, we return to the long term goal of this work and note that implementation of these VPLW type methods will be done for the nonlinear gas dynamic equations solved on Lagrangian meshes. As previously discussed, the RR method and its offshoots are well suited to such an extension. Care has been taken to ensure that the VPFCT algorithm retains this suitability.

ACKNOWLEDGEMENTS

The authors would like to acknowledge the following organizations for their generous support of this research. The first author would like to thank The Department of Defense High Performance Computing Modernization Office through a National Defense Science and Engineering Graduate (NDSEG) Fellowship, AWE Aldermaston for facilitating a visit to the Centre for Scientific Computing at the University of Cambridge where some of this work was performed, and The Methods and Algorithms group at Los Alamos National Laboratory, Contract 123139. The second author would like to thank AWE Aldermaston through the William Penney Professorship. We wish to thank the two anonymous referees for their close and thoughtful readings of our first draft.

REFERENCES

1. Wilkins ML. Calculation of elastic-plastic flow. In *Methods in Computational Physics*, Vol. 3. Academic Press: New York, 1964; 211-263.
2. Caramana EJ, Burton DE, Shashkov MJ, Whalen PP. The construction of compatible hydrodynamics algorithms utilizing conservation of total energy. *Journal of Computational Physics* 1998; **146**:227–262.
3. Després B, Mazeran C. Lagrangian gas dynamics in two dimensions and Lagrangian systems. *Archive for Rational Mechanics and Analysis* 2005; **178**:327–372.
4. Maire PH, Abgrall R, Breil J, Ovadia J. A cell-centered Lagrangian scheme for two-dimensional compressible flow problems. *SIAM Journal on Scientific Computing* 2007; **29**(4):1781–1824.
5. Maire PH, Breil J. A second-order cell-centered Lagrangian scheme for two-dimensional compressible flow problems. *International Journal for Numerical Methods in Fluids* 2008; **56**:1417–1423.
6. Carré G, Del Pino S, Després B, Labourasse E. A cell-centered Lagrangian hydrodynamics scheme on general unstructured meshes in arbitrary dimensions. *Journal of Computational Physics* 2009; **228**:5160–5183.
7. Barlow AJ, Roe PL. A cell centred Lagrangian Godunov scheme for shock hydrodynamics. *Computers and Fluids* 2011; **46**(1):133–136.
8. Burton DE, Carney TC, Morgan NR, Sambasivan SK, Shashkov MJ. A cell-centered Lagrangian Godunov-like method for solid dynamics. *Computers and Fluids* 2013; **83**:33–47.
9. Dukowicz JK, Cline MC, Addessio FS. A general topology Godunov method. *Journal of Computational Physics* 1989; **82**:29–63.
10. Morton KW, Roe PL. Vorticity-preserving Lax-Wendroff-type schemes for the system wave equation. *SIAM Journal on Scientific Computing* 2001; **23**(1):170–192.
11. Jeltsch R, Torrilhon M. On curl-preserving finite-volume discretizations for the shallow-water equations. *BIT Numerical Mathematics* 2006; **46**:S35–S53.
12. Mishra S, Tadmor E. Vorticity-preserving schemes using potential-based fluxes for the system wave equation. *Proceedings of Symposia in Applied Mathematics* 2009; **67**(2):795–804.
13. Bauer AL, Loubère R, Wendroff B. On stability of staggered schemes. *SIAM Journal on Numerical Analysis* 2008; **46**(2):996–1011.
14. Wilson JC. Stability of Richtmyer type difference schemes in any finite number of space variables and their comparison with multistep Strang schemes. *IMA Journal of Applied Mathematics* 1972; **10**(2):238–257.
15. Turkel E. Phase error and stability of second order methods for hyperbolic problems I. *Journal of Computational Physics* 1974; **15**:226–250.
16. Dukowicz JK, Meltz BJA. Vorticity errors in multidimensional Lagrangian codes. *Journal of Computational Physics* 1992; **99**:115–134.
17. Toro EF. In *Riemann Solvers and Numerical Methods for Fluid Dynamics: A practical Introduction*. Springer: Berlin, 2009; 561–563.
18. Lax P, Wendroff B. Systems of conservation laws. *Communications on Pure and Applied Mathematics* 1960; **13**: 217–237.

DOI: 10.1002/fld

19. Lax P, Wendroff B. Difference schemes for hyperbolic equations with high order of accuracy. *Commmunications on Pure and Applied Mathematics* 1964; **17**:381–398.
20. Strang G. Accurate partial difference methods II. Non-linear problems. *Numerische Mathematik* 1964; **6**:37–46.
21. Gottlieb D, Turkel E. Phase error and stability of second order methods for hyperbolic problems II. *Journal of Computational Physics* 1974; **15**:251–265.
22. Lukáčová-Medvid'ová M, Morton KW, Warnecke G. Evolution Galerkin methods for hyperbolic systems in two space dimensions. *Mathematics of Computation* 2000; **69**(232):1355–1384.
23. Vichnevetsky R, Bowles JB. In *Fourier Analysis of Numerical Approximations of Hyperbolic Equations*. SIAM: Philadelphia, 1982; 115–129.
24. Kumar A. Isotropic finite differences. *Journal of Computational Physics* 2004; **201**(1):109–118.
25. Zalesak ST. The design of flux-corrected transport (FCT) algorithms for structured grids. In *Flux-Corrected Transport*. Springer: Berlin, 2005; 29–78.
26. Friedrichs KO. Symmetric hyperbolic linear differential equations. *Communications on Pure and Applied Mathematics* 1954; **7**:345–392.
27. Boris JP, Book DL. Flux-corrected transport I: SHASTA, a fluid transport algorithm that works. *Journal of Computational Physics* 1973; **11**:38–69.
28. Liu X-D, Lax P. Positive schemes for solving multi-dimensional systems of hyperbolic conservation laws. *CFD Journal* 1996; **5**(2):133–156.
29. van Leer B. Toward the ultimate conservative difference scheme I. The quest of monotonicity. In *Proceedings of the Third International Conference on Numerical Methods in Fluid Mechanics*. Springer: Berlin Heidelberg, 1973; 163–168.
30. Boris JP, Book DL. Flux-corrected transport III: Minimal-error FCT algorithms. *Journal of Computational Physics* 1976; **20**:397–431.
31. Boris JP, Book DL, Hain K. Flux-corrected transport II: Generalizations of the method. *Journal of Computational Physics* 1975; **18**:248–283.
32. Zalesak ST. Fully multidimensional Flux-corrected Transport algorithms for fluids. *Journal of Computational Physics* 1979; **31**:335–362.

DOI: 10.1002/fld